Received: 5 July 2019 | Accepted: 3 February 2020

DOI: 10.1002/hyp.13720

RESEARCH ARTICLE

WILEY

Assimilating snow observations to snow interception process simulations

Zhibang Lv | **John W. Pomeroy**

Centre for Hydrology, University of Saskatchewan, Saskatoon, Canada

Correspondence
Zhibang Lv, 101-121 Research Dr. Saskatoon, SK S7N 1K2, Canada.
Emai:
Email: zhibang.lv@usask.ca

Funding information
Alberta Agriculture and Forestry; Alberta Innovates; Canada Research Chairs Program; Natural Sciences and Engineering Research Council of Canada; the Global Water Futures Program; Canada Excellence Research Chair in Water Security; Changing Cold Regions Network

Abstract

Snow interception is a crucial hydrological process in cold regions needleleaf forests, but is rarely measured directly. Indirect estimates of snow interception can be made by measuring the difference in the increase in snow accumulation between the forest floor and a nearby clearing over the course of a storm. Pairs of automatic weather stations with acoustic snow depth sensors provide an opportunity to estimate this, if snow density can be estimated reliably. Three approaches for estimating fresh snow density were investigated: weighted post-storm density increments from the physically based Snobal model, fresh snow density estimated empirically from air temperature (Hedstrom, N. R., et al. [1998]. *Hydrological Processes*, *12*, 1611–1625), and fresh snow density estimated empirically from air temperature and wind speed (Jordan, R. E., et al. [1999]. *Journal of Geophysical Research*, 104, 7785–7806). Automated snow depth observations from adjacent forest and clearing sites and estimated snow densities were used to determine snowstorm snow interception in a subalpine forest in the Canadian Rockies, Alberta, Canada. Then the estimated snow interception and measured interception information from a weighed, suspended tree and a time-lapse camera were assimilated into a model, which was created using the Cold Regions Hydrological Modelling platform (CRHM), using Ensemble Kalman Filter or a simple rule-based direct insertion method. Interception determined using density estimates from the Hedstrom-Pomeroy fresh snow density equation agreed best with observations. Assimilating snow interception information from automatic snow depth measurements improved modelled snow interception timing by 7% and magnitude by 13%, compared to an open loop simulation driven by a numerical weather model; its accuracy was close to that simulated using locally observed meteorological data. Assimilation of tree-measured snow interception improved the snow interception simulation timing and magnitude by 18 and 19%, respectively. Time-lapse camera snow interception information assimilation improved the snow interception simulation timing by 32% and magnitude by 7%. The benefits of assimilation were greatly influenced by assimilation frequency and quality of the forcing data.

KEYWORDS

CRHM, data assimilation, EnKF, fresh snow density, GEM, modelling, snow depth, Snow interception

1 | INTRODUCTION

The seasonal snowcover strongly influences cold regions hydrological cycles and energy budgets through its storage of precipitation, temperature at or below 0°C and relatively high albedo. The processes governing snow dynamics in cold regions needleleaf forests, which cover more than 20% of the Earth's land surface, are very different from open areas because the forest canopy alters snow and energy distribution (Pomeroy et al., 2008; Pomeroy & Gray, 1995; Suzuki & Nakai, 2008). In needleleaf forests, some snowfall is usually intercepted by the forest canopy where it can be stored up to months at a time (Pomeroy & Schmidt, 1993). This intercepted snow can then unload, melt, or sublimate (Pomeroy & Goodison, 1997). Snow interception and release from forest canopies are mainly controlled by the depth of snowfall, air temperature, humidity, wind speed, and canopy structure (Hedstrom & Pomeroy, 1998; Storck, Lettenmaier, & Bolton, 2002; Pomeroy, Gray, Hedstrom, & Janowicz, 2002). Snow interception leads to snow accumulation on the forest floor being notably different from nearby open areas. Studies have reported that up to 60% annual snowfall can be intercepted by the canopy and two thirds of that snow never reaches the ground due to sublimation (Kuz'min, 1960; Pomeroy & Schmidt, 1993; Storck et al., 2002). Due to snow's high albedo, relatively cold temperature and low thermal conductivity, it affects energy partitioning in and beneath the canopy (Suzuki & Nakai, 2008). Snowmelt runoff from the Canadian Rockies contributes to the headwaters of major rivers that supply water to large portions of western Canada and the northwestern United States. Needleleaf forests cover much of the Canadian Rockies, and so accurate determination of the magnitude and timing of snow interception plays an important role in regional water management (Lv, Pomeroy, & Fang, 2019; Pomeroy, Fang, & Ellis, 2012).

Numerous methods have been developed in recent decades to quantitatively or qualitatively measure intercepted snow (cf. Friesen, Lundquist, & Van Stan, 2015). Mass budgeting, which examines the snow accumulation or snowfall difference between forest floor and open areas over the course of a snowstorm, is the most common indirect approach for quantitatively estimating snow interception (Pomeroy & Gray, 1995). Precipitation or snow accumulation can be measured by using traditional precipitation gauges (Koivusalo & Kokkonen, 2002), artificial boards (e.g., Floyd & Weiler, 2008; Lundberg, Calder, & Harding, 1998), or snow surveys (Hedstrom & Pomeroy, 1998). The annual loss caused by sublimation of intercepted snow can be obtained by difference in the peak SWE between an adjacent forest and open area (Lundberg et al., 1998; Pomeroy & Schmidt, 1993; Winkler, Spittlehouse, & Golding, 2005). The direct approach for measuring snow interception on a single tree or branch involves a weighing scale or compression sensor that connects to a cut, a live tree or branch to measure weight change during and after a snow storm (Hedstrom & Pomeroy, 1998; Lundberg et al., 1998; Martin et al., 2013; Pomeroy & Schmidt, 1993; Schmidt & Pomeroy, 1990; Suzuki & Nakai, 2008). Although these approaches can provide accurate interception measures, they all have drawbacks. For example, a cut suspended tree (branch) dries out in time changing its tare weight. The compression sensor method is still experimental. Images from ground based digital cameras (Floyd & Weiler, 2008; Garvelmann, Pohl, & Weiler, 2013; Pomeroy & Schmidt, 1993) or an optical remote sensing satellite (Lv & Pomeroy, 2019) have been used to detect canopy snow presence based on the high reflectance of snow. Some of these studies have developed methods to calculate the canopy snow-covered area of the canopy; however, the actual amount of intercepted snow has remained elusive. Snow mass budgeting is laborious and requires regular observations to determine field SWE changes. Automatic snow accumulation measurements are not readily available, or possible, under forest canopies in most cold regions (Kinar & Pomeroy, 2015). Nevertheless, automatic, ultrasonic snow depth sensors are usually included in automated meteorological stations. Snow depth measurements like this have been used to derive solid precipitation (Mair et al., 2016), snow density (Helfricht, Hartl, Koch, Marty, & Olefs, 2018), and snow accumulation as snow water equivalent or SWE (Egli, Jonas, & Meister, 2009), and have been used to compare water balance between forests and clearings (Bales et al., 2011). However, their use to quantitatively determine snow interception needs to be further explored.

Many models have been developed to simulate snow interception and unloading in forests (e.g., Bartlett, MacKay, & Verseghy, 2006; Hedstrom & Pomeroy, 1998; Niu & Yang, 2004). In these models, interception is usually determined by the initial snow load, snowfall rate, and the maximum snow storage capacity of the canopy, which is determined by air temperature, fresh snow density, and canopy coverage. The unloading of intercepted snow is usually determined by wind speed and time since snowfall. Intercepted snow changes both the albedo and canopy temperature (Lv & Pomeroy, 2019), hence alters the shortwave and longwave radiation around the canopy to varying degrees (Pomeroy & Dion, 1996). Because volumes of canopy intercepted snow are relatively smaller than snow on the ground and intercepted snow remains in the canopy over time periods from a few hours to a few months, canopy snow modelling is more sensitive than ground snowpack to the quality of the forcing data. However, because of sparse meteorological observations in cold regions forests, climate model outputs, that have relatively lower accuracy, are the only available data source to model snow interception in most areas. Hence, there is a need for data assimilation (DA) to allow better simulation of snow interception.

Both observations and models have drawbacks when estimating snow interception. Observations are usually limited by small spatial coverage (e.g., weighed suspended tree lysimetry) or sparse repeat frequency (e.g., satellite remote sensing), or both (e.g., manual snow survey). Models are simplified representations of real-world physical processes and their simulation accuracy is greatly influenced by the quality of parameterization and input data. To optimize estimation of hydrological properties, DA has been introduced to hydrological models to combine the advantages of observations (e.g., relatively higher accuracy) and models (e.g., low cost and consistent at reasonable spatial and temporal scales).

Many DA methods have been developed in environmental science, which vary in how they treat observations and model simulation error covariance (Liu et al., 2012). Simple insertion methods assume that observations are perfect and only models contain error. Hence, modelled state variables are directly replaced by observations whenever there is an observation available. Other DA approaches that adopt improved sophisticated algorithms to determine model and observational uncertainty have being used by many cold regions hydrologists. The most common are the Kalman filter (KF) family (traditional KF, EKF, EnKF), Particle Filter (PF), and four-dimensional variational data assimilation (4DVAR). Cold regions hydrologists have used these approaches to assimilate both *in situ* observations and remotely sensed data, including snow cover fraction (Andreadis & Lettenmaier, 2006; Clark et al., 2006; De Lannoy et al., 2012; Liu et al., 2013; Rodell & Houser, 2004; Slater & Clark, 2006; Stigter et al., 2017), snow depth (Hedrick et al., 2018; Kumar et al., 2014; Kumar, Dong, Peters-Lidard, Mocko, & Gómez, 2017; Liu et al., 2013; Lv, 2019; Magnusson, Winstral, Stordal, Essery, & Jonas, 2017; Stigter et al., 2017), and SWE (Andreadis & Lettenmaier, 2006; Bergeron, Trudel, & Leconte, 2016; Franz, Hogue, Barik, & He, 2014; Huang, Newman, Clark, Wood, & Zhang, 2017; Liston & Hiemstra, 2007; Lv, 2019), into hydrological models. However, to authors' knowledge, the assimilation of snow interception information has yet to be explored.

The principal aim of this study is to use DA to improve snow interception process simulations that are forced by uncertain atmospheric model outputs. This research first studied the use of automatically measured snow depth from adjacent forest and clearing sites to quantitatively estimate snow interception in a headwater basin in the Canadian Rocky Mountains. Then, these snow interception data, along with a weighed, suspended tree and time-lapse camera measured snow interception information, were assimilated into a physically based, process-hydrology Cold Regions Hydrological Modelling platform (CRHM) forcing by uncertain atmospheric model outputs using EnKF and rule based direct insertion to achieve the goal of improving snow interception process simulations through DA. Specific research objectives are 1) to determine how automatically measured snow depth in forests and adjacent clearings can be used to quantify snow interception loss in the forest, and, 2) to examine the influence of assimilating ground measured and remotely sensed snow interception information on snow interception process simulations.

2 | STUDY AREA AND DATA

2.1 | Marmot Creek Research Basin

This study took place in the Upper Forest (UF) and Upper Clearing (UC) sites at the Marmot Creek Research Basin (MCRB). MCRB is located in the Front Ranges of the Canadian Rockies in Alberta, Canada (Figure 1). The basin area is approximately 9.4 km^2 and basin elevations range from 1,700 to 2,825 m. At low to middle elevations, continuous stands of Lodgepole Pine, Engelmann Spruce, and Douglas-fir are the dominant tree species. Upper elevations are dominated by Larch, Engelmann Spruce, Subalpine Fir, shrubs, and grasses. The highest elevations are covered largely by talus and exposed rock. The main precipitation type in the basin is snowfall (up to 75% in high elevations) with mean annual precipitation varying by elevation from 660 to 1,140 mm. Approximately 65% of basin is covered by dense forest resulting in snow interception playing a crucial role in snow accumulation dynamics in the basin (Lv et al., 2019). Snow interception by the forest canopy and sublimation of intercepted snow both control snow accumulation such that up to 60% of the annual snowfall never reaches the ground under the needleleaf forests (Ellis, Pomeroy, Brown, & MacDonald, 2010). In the 1970s, six large and thousands of small clearings were cut to study the influence of deforestation on local hydrology (Rothwell, Hillman, & Pomeroy, 2016). UC is located at a middle elevation (1840 m) clearing with a diameter of approximately 60 m. Forty years after deforestation, the main vegetation type in UC is short grass and natural forest regrowth with young trees less than 2 m high. The UF site is located in a relatively level mature mixed forest stand of Spruce, Fir and Pine that is approximately 30 m from the northwest edge of UC.

2.2 | Data collection

Two meteorological stations were erected in 2005 at UC and UF to continuously measure climate data (15-min intervals). In addition to standard meteorological sensors, the stations consisted of a snow depth sensor (Campbell Scientific SR50) and a weighing precipitation gauge (Alter-shielded Geonor) to measure precipitation (UC only). Precipitation data were corrected for wind-induced undercatch (Smith, 2009). Hourly air temperature, relatively humidity, soil temperature, wind speed, short- and longwave radiation, snow depth, and precipitation data until September 2017 were collected at both sites (Fang, Pomeroy, DeBeer, Harder, & Siemens, 2019).

In addition to locally observed meteorological data, the Environment and Climate Change Canada Global Environmental Multiscale (GEM) model 2.5 km grid product from November 2014 to August 2017 was used to run the CRHM model for DA experiments. Four grids of GEM data were needed to cover the entire MCRB basin. GEM outputs were hourly air temperature, relative humidity, wind speed, incoming shortwave radiation, incoming longwave radiation, and precipitation. These outputs were not bias corrected. The 2.5 km GEM data were downscaled to Hydrological Response Unit (HRU, which is the basic simulation unit in CRHM) scale before forcing CRHM. Precipitation and air temperature for each HRU were adjusted based on the observed elevation lapse rate in MCRB. Other forcing variables of each HRU were assigned to the value of the closest GEM grid cell.

A freshly cut, mature, full-size tree was suspended and weighed at UF to quantitatively measure snow interception on forest canopy

from January 2016 to June 2017 using the technique of Hedstrom and Pomeroy (1998). A time-lapse camera (Wingscapes Timelapse-Cam) was mounted on the Gold Chair lift at the Nakiska Ski Resort beside MCRB from March 2015 to June 2016 to take hourly pictures of the forest canopy in the basin.

Snow surveys were conducted one to three times each month at both sites from November to June of each hydrological year from 2006 to 2017. The survey follows designed transects near the sites with at least 25 snow depth measures and one snow density measure among every five depth measurements using an ESC30 snow tube.

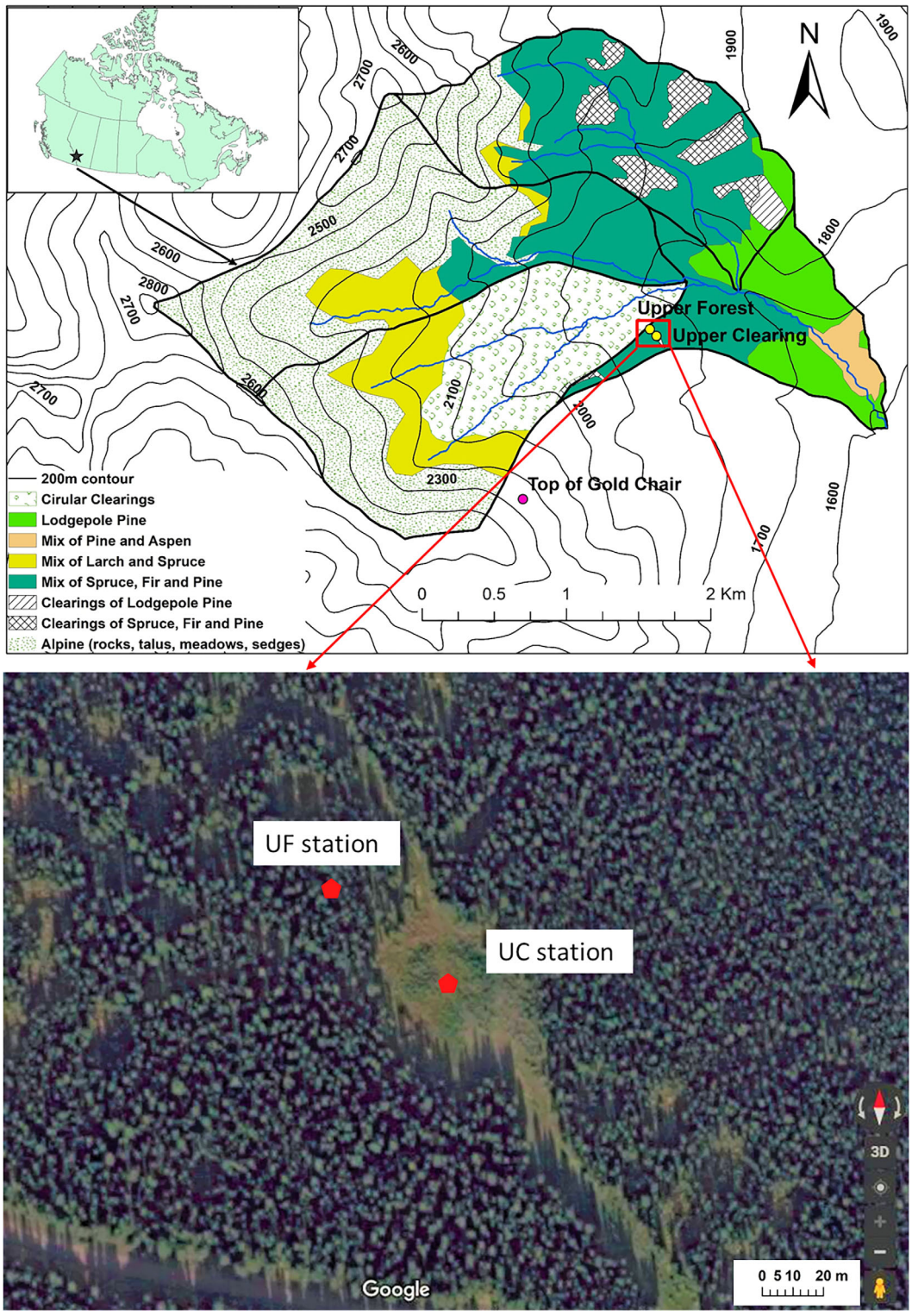

FIGURE 1 Landscape of Marmot Creek Research Basin, Alberta, Canada (top) and a close-up of upper forest and upper clearing sites (bottom, photo from Google Map)

3 | METHODS

3.1 | Snow interception estimation

In this research, snow interception data from three sources (suspended tree, time-lapse camera, and automatic snow depth measurement) were used. Hourly images from the time-lapse camera were processed following Lv and Pomeroy (2019) to determine the time of intercepted snow on the forest canopy. To obtain areal scale snow interception magnitude for each snow storm using the automatic snow depth measurement, three fresh snow density estimation methods (see Section 3.1.2) were applied covert the upscaled automatic measured snow depth change (see Section 3.1.1) to SWE change during each snow storm. Then, forest canopy snow interception at the UF site was determined by the difference between SWE changes in UC and UF during each snow event using Equation (1):

$$\mathrm{Int} = \Delta\mathrm{SWE}_{\mathrm{UC}} - \Delta\mathrm{SWE}_{\mathrm{UF}}, \quad (1)$$

where Int is the snow interception (mm) for a snowfall event in UF, $\Delta\mathrm{SWE}_{\mathrm{UC}}$ and $\Delta\mathrm{SWE}_{\mathrm{UF}}$ denote the SWE change (mm) during the snow fall for UC and UF, respectively.

The estimated snow interception data from the three methods were compared to the snow interception measured by the suspended tree at UF from January 2016 to June 2017 to determine the optimal method of snow interception estimation using automated snow depth measurement at the study site.

The suspended tree only measured interception amount at the single tree scale, while the interception data obtained from snow survey transects were for areal scale. Snow interception estimated from the snow surveys was then used to upscale the tree measurement to areal scales based on the linear relationship between the two data sets as per Hedstrom and Pomeroy (1998). The suspended tree branch and needle area changed each winter as a fresh tree was deployed in the fall and so this scaling was recalculated every year to achieve the best results.

3.1.1 | Snow depth data filtering

SR50-measured fixed point snow depth data usually contain error and noise and are unable to represent landscape mean (Neumann, Derksen, Smith, & Goodison, 2006; Ryan, Doesken, & Fassnacht, 2008). Therefore, the data were error corrected, smoothed, and upscaled following the methods in Lv (2019). Because air temperature influences the speed of sound, temperature compensation was conducted on SR50 ultrasonic sensor reading according the following formula provided by Campbell Scientific (2009):

$$S_c = S_r\sqrt{\frac{T_a}{273.15}}, \quad (2)$$

where S_c is the compensated snow depth, S_r is the raw SR50 sensor reading, and the T_a is air temperature in Kelvin.

After compensation, snow depth data still contains noise. "Noisy" data were removed by applying a three-hour moving average following Ryan et al. (2008). Fixed point snow depth measurements usually systematically over- or under-estimate areal means because of heterogeneity in snow accumulation, redistribution, and ablation caused by topography, vegetation and wind (Pomeroy & Gray, 1995). Therefore, these were upscaled using a "scaling equation" developed using the relationship between temperature compensated, noise removed SR50 data and areal mean snow depth data from snow surveys at each site. For details of these "scale equations" refer to Lv (2019).

3.1.2 | Fresh snow density estimation

Three methods were used to estimate fresh snow density to calculate SWE from the SR50 snow depth data. Because of the popularity of airborne snow depth measurements, many studies have combined them with simulated snow density to estimate SWE in cold regions (Hedrick et al., 2018; Painter et al., 2016). In the present research, the first method used the physically based energy-balance Snobal module in CRHM, running local observed meteorological data to simulate the snowpack density. However, Snobal can only simulate the density for an entire snowpack. Pomeroy and Gray (1995) reported that different snow densities should be applied to fresh and old snow. Concomitant increases of simulated SWE and snow depth during snowfall events were used to calculate fresh snow density. The second method is described in Equation (3), proposed by Hedstrom and Pomeroy et al. (1998), that uses air temperature to calculate freshly fallen snow density (the Hedstrom-Pomeroy method hereafter).

$$\rho_{fs} = 67.9 + 51.3\,e^{T/2.6}, \quad (3)$$

where ρ_{fs} is the fresh fallen snow density, T is the air temperature at 2 m (°C).

The third method is described by Equation (4), developed by Jordan, Andreas, and Makshtas (1999), that uses air temperature and wind speed to estimate freshly fallen snow density (the Jordan et al. method hereafter).

$$\begin{cases} \rho_{fsJ} = 500\left[1 - 0.951e^{\left(-1.4(278.15-(T+273.15))^{-1.15} - 0.008u^{1.7}\right)}\right] & -13 < T \le 2.5^{\circ}C \\ \rho_{fsJ} = 500\left[1 - 0.904e^{\left(-0.008u^{1.7}\right)}\right] & T \le -13^{\circ}C \end{cases}, \quad (4)$$

where u is the 10-m wind speed in m/s.

Because the snowpack densification rate in cold and sheltered environments is usually as low as 25 kg/m^3 per month during the winter (Pomeroy et al., 1998), all three methods assumed that the densification of the lower, old snowpack is negligible during snowfall events and the change of snowpack depth is the contribution of fresh snow alone. The second and the third methods assume that fresh snow densities in the clearing and the forest are same during the snowstorm.

Snowfall events with mixed precipitation types (snow and rain) can affect the accuracy of snow density estimation. Thus, data from these storms were excluded from analyses and only data from pure snow storms were analyzed. The precipitation phase of an event was determined following the psychrometric energy budget method proposed by Harder and Pomeroy (2013).

Measured snowfall from a shielded weighing precipitation gauge and snow depth increase were used to estimate the actual fresh snow density of each storm. These data were used to validate the calculated fresh snow density using root mean square error (RMSE, Equation (5)) and Model Bias (MB, Equation (6)).

$$\mathrm{RMSE} = \sqrt{\frac{\sum_{i=1}^{n}(Xo_i - Xs_i)^2}{n}}, \tag{5}$$

$$\mathrm{MB} = \frac{\sum Xs}{\sum Xo} - 1, \tag{6}$$

where x_s and x_o are simulated and observed fresh snow density, respectively.

3.2 | Cold Regions Hydrological Model platform

The Cold Regions Hydrological Model platform (CRHM) was used to create a model to simulate snow interception and release from the forest canopy at the UF site. CRHM is a modular platform designed to assemble custom hydrological models that are suitable for cold regions. Researchers can create projects by choosing from a wide range of basin configurations, spatial and temporal resolutions, and hydrological process modules based on their research interests, data availability, and research basin scale. The CRHM library contains many modules that can be used to interpolate meteorological data, simulate rainfall and snowfall interception, wind redistribution, sublimation, albedo decay, canopy transmittance, snow energy and mass balance, evaporation, melt, snowcover depletion, infiltration, soil moisture, flow and storage of surface and subsurface, and streamflow routing. Detailed information about CRHM and the modules are given in several recent publications (Ellis et al., 2010; Fang et al., 2013; Fang & Pomeroy, 2016; Pomeroy et al., 2007; Pomeroy, Fang, & Marks, 2016).

The canopy module used in this study was initially developed by Parviainen and Pomeroy (2000) and later modified by Ellis et al. (2010). The main parameters of this module are canopy snow-free albedo, leaf area index (LAI), maximum canopy snow interception load, ice bulb temperature that controls snow unloading as solid or liquid, and the measurement height of air temperature and wind speed. These parameters were set according to field measurements or following the research of Ellis et al. (2010) and Pomeroy et al. (2012).

The Snobal module (Marks, Kimball, Tingey, & Link, 1998; DeBeer & Pomeroy, 2010) was used to simulate the snowpack mass - energy balance and the snow density on the ground. Snobal assumes fresh fallen snow density as 100 kg/m^3. It divides the snowpack into two layers (active and lower) that share the same density. The active layer has a maximum thickness of 10 cm following Marks et al. (2008). The forcing data for the model are locally observed or GEM produced air temperature, relative humidity, soil temperature, wind speed, incoming shortwave radiation, and precipitation. The model is flexible but in this case was run at an hourly time step. When observations become available, model runs stop at 1 a.m. and a state file is exported. This state file contains values of all necessary state variables and fluxes at that moment. After the assimilation, this file is updated and set as the initial condition for next model run.

3.3 | Snow interception assimilation

In the present research, three snow interception data sets were assimilated into CRHM to evaluate the influence of DA on snow interception process simulations. The Ensemble Kalman Filter (EnKF) was used to assimilate snow interception data obtained by snow depth measurements and suspended tree at the UF site. Because EnKF is only able to assimilate continuous data, a rule based simple insertion method was used to assimilate the time-lapse camera measured snow interception information.

3.3.1 | Ensemble Kalman Filter

EnKF is a sequential assimilation approach that can be used to update model state variable(s) whenever an observation is available. It was chosen because it is straightforward to implement and has been successful worldwide to assimilate other snow properties into hydrological models (e.g., Franz et al., 2014; He, Hogue, Margulis, & Franz, 2012; Kumar, Koster, Crow, & Peters-Lidard, 2009). The updating quantity is determined using the Kalman gain (K, Equation (7)), which is calculated from the error covariance of ensemble model simulations and observations, and the difference between simulated and observed state variable (Equation (8)).

$$K_i = \frac{P_i^s}{H_i P_i^s + R_i}, \tag{7}$$

where P_i^s and R_i are the forecast model and observation error covariances at time step i, respectively. Model forecast error covariance is calculated from the ensemble model simulation covariance at each time step. The observation error covariance of step i is represented by the error covariance of ensemble observations perturbed from observation i with a presumed standard deviation.

$$x_{i,j}^a = x_{i,j}^b + K_i\left(y_{i,j} - H_i x_{i,j}^b\right), \tag{8}$$

where $x_{i,j}$ and $y_{i,j}$ are the j^{th} (j = 1, 2, …, N, N is ensemble size) ensemble model state and observation vector, respectively, at time step

i (i = 1, 2, …, M, M is number of observations); superscripts a and b represent the model state vectors after and before the update. H_i is the observation operator that relates the model vector to the observed vector and it is a unit factor in this study as the model vector and observed vector are same.

Uncertainty in simulating snow interception was assumed to be primarily caused by uncertainty in forcing atmospheric data. Therefore, ensemble model simulations were run using Monte Carlo perturbed forcing data following an approach used in many studies (Kumar et al., 2014; Liu et al., 2013; Reichle, Walker, Koster, & Houser, 2002; Table 1). The multiplicative perturbation, with a mean value of 1 and presumed standard deviation (SD), was performed to incoming shortwave radiation (SD = 0.3) and precipitation (SD = 0.5). This perturbation can avoid unreasonable outcomes such as negative precipitation or positive incoming short-wave radiation at night. For other driving forces, additive perturbation with a mean value of zero was run (Table 1). For the model state variable (canopy snow load) multiplicative perturbation was conducted, with a mean value of 1 and a SD of 0.05.

Forcing variables are frequently related, such as higher air temperature often resulting in lower relative humidity. A cross correlation was performed for all forcing variables except wind speed using established relationships (De Lannoy et al., 2012; Reichle et al., 2007) (Table 1). Theoretically, more ensemble simulations in EnKF DA means higher accuracy. However, in consideration of computational efficiency, 20 was chosen as an ensemble number following existing research (Kumar et al., 2009; Kumar et al., 2014) and experience. Using EnKF, snow interception data derived from SR50 measurement was assimilated for each snow storm detected from November 2014 to August 2017 (hereafter DA_SR50). The suspended tree measured snow interception was assimilated daily from January 2016 to June 2017 (hereafter DA_Tree).

3.3.2 | Rule-based direct insertion

Although snow interception data derived from the time-lapse camera (TLC) and satellite images are not able to determine the magnitude of interception, they do provide interception timing. In particular, the data from the time-lapse camera not only provides snowfall initiation, but also duration of snow interception storage on the canopy. To assimilate this information into CRHM, a rule based simple insertion method inspired by the satellite measured snowcover information assimilation research of Rodell and Houser (2004) and Liu et al. (2013), was proposed. TLC-derived snow interception information was assimilated daily (hereafter DA_TLC). Simulated snow interception was compared to the TLC information at end of each day. If model-simulated snow interception was less than 1 mm and TLC information indicated there was snow on the canopy, snow interception was adjusted to a minimum value (3 mm). This value was chosen because it is close to average interception (3.5 mm) for snow storms at the study site. However, if model-simulated snow interception was greater than 1 mm but TLC information indicated there was no snow on the canopy, the simulated snow was adjusted to 0. Assimilation can be only conducted at midnight on each day in CRHM, but TLC can only show interception information during daylight. Hence, there were several hours of lag between the observation and assimilation time. In addition, snowfall and intercepted snow unloading can occur at night. Therefore, only days with obvious midnight snow interception information were assimilated. On such days, canopy snow interception information consisted of before sunset of the first day and after sunrise of the second day. Therefore, days with nighttime snowfall, but unknown midnight snow interception information, indicated by no snow on the canopy in the evening but snow present on the canopy the following day, were omitted from the assimilation process.

3.3.3 | Data assimilation evaluation

In addition to the three DA experiments, two open loop (OL) experiments without DA were conducted to assess the influence of DA on interception simulation. One was forced by GEM data (GEM_OL) and the other was forced by local observed meteorological data (ObsMet). The accuracy of each simulation was assessed using the magnitude and timing of interception. The accuracy of simulated interception magnitude of each OL and DA experiment was evaluated using

TABLE 1 Model driving and state variables with perturbation parameters

Variables			Cross correlations with perturbations					
Forcing variables	**Perturbation type**	**Standard deviation**	**AT**	**RH**	**u**	**SW**	**LW**	**P**
Air temperature (AT)	Additive	5°C	1	−0.3	-	0.3	0.6	−0.1
Relative humidity (RH)	Additive	10	−0.3	1	-	−0.8	0.5	0.8
Wind speed (u)	Additive	2 m/s	-	-	1	-	-	-
incoming short-wave radiation (SW)	Multiplicative	0.3	0.3	−0.8	-	1	−0.3	−0.5
incoming long-wave radiation (LW)	Additive	50 (W/m^2)	0.6	0.5	-	−0.3	1	0.5
Precipitation (P)	Multiplicative	0.5	−0.1	0.8	-	−0.5	0.5	1
CRHM state variables			SWE					
Intercepted SWE	Multiplicative	0.05	1					

the RMSE (Equation (5)) between these simulations and suspended tree measurements. For timing, the duration of intercepted snow (hours) for each experiment was calculated and normalized to the duration of intercepted snow derived from time-lapse photography.

4 | RESULTS

4.1 | Snow depth in forest and clearing

According to SR50 measurements, snow depth in the clearing was frequently higher than that in the forest (Figure 2). For the 12 hydrological years of observations, annual peak snow depth in the clearing and forest were correlated (r^2 = 0.91, p < 0.05). Peak snow depth in the forest was 26.5–54.1% (mean: 45.8%) less than that in the clearing. At the end of the snow season, the snowpack on the ground has a 0 to 8 day longer duration (mean: 4.4 days) in the forest than in the clearing. Snow survey data indicated that snowpack density in the clearing and forest were correlated, but not strongly (r^2 = .5, p < .05; Figure 3a) and the snowpack density distribution and mean value at the two sites were similar (Figure 3b). A t-test for the two data sets found no significant difference between snow density sample means from the clearing and forest (data not shown). Therefore, the SWE ratio can be considered to be equal to the snow depth ratio between the two sites.

Snow depth increases during snowfall events at UC and UF were strongly correlated (r^2 = .9, p < .05), with a significant linear relationship (Figure 4). On average, snow depth increases in the forest were approximately 47.6% lower than those in the clearing. For several small events, snow depth changes in the forest were negative even though there was a snow depth increase at UC. This can be explained by high interception efficiency for low snowfall amounts such that there was little accumulation below the canopy. Minor densification (<3 cm) also affects the old snowpack depth on the forest floor during the event. Almost all the events with heavy snow (snow depth increase greater than 30 cm in UC) were located above the correlation line, demonstrating that the snow interception efficiency decreases whilst snowfall amount increases.

4.2 | Fresh snow density estimation

Snobal-simulated snowpack density was compared to directly observed snowpack density at UC and UF from 2005 to 2017. The model simulation frequently overestimated observed snowpack

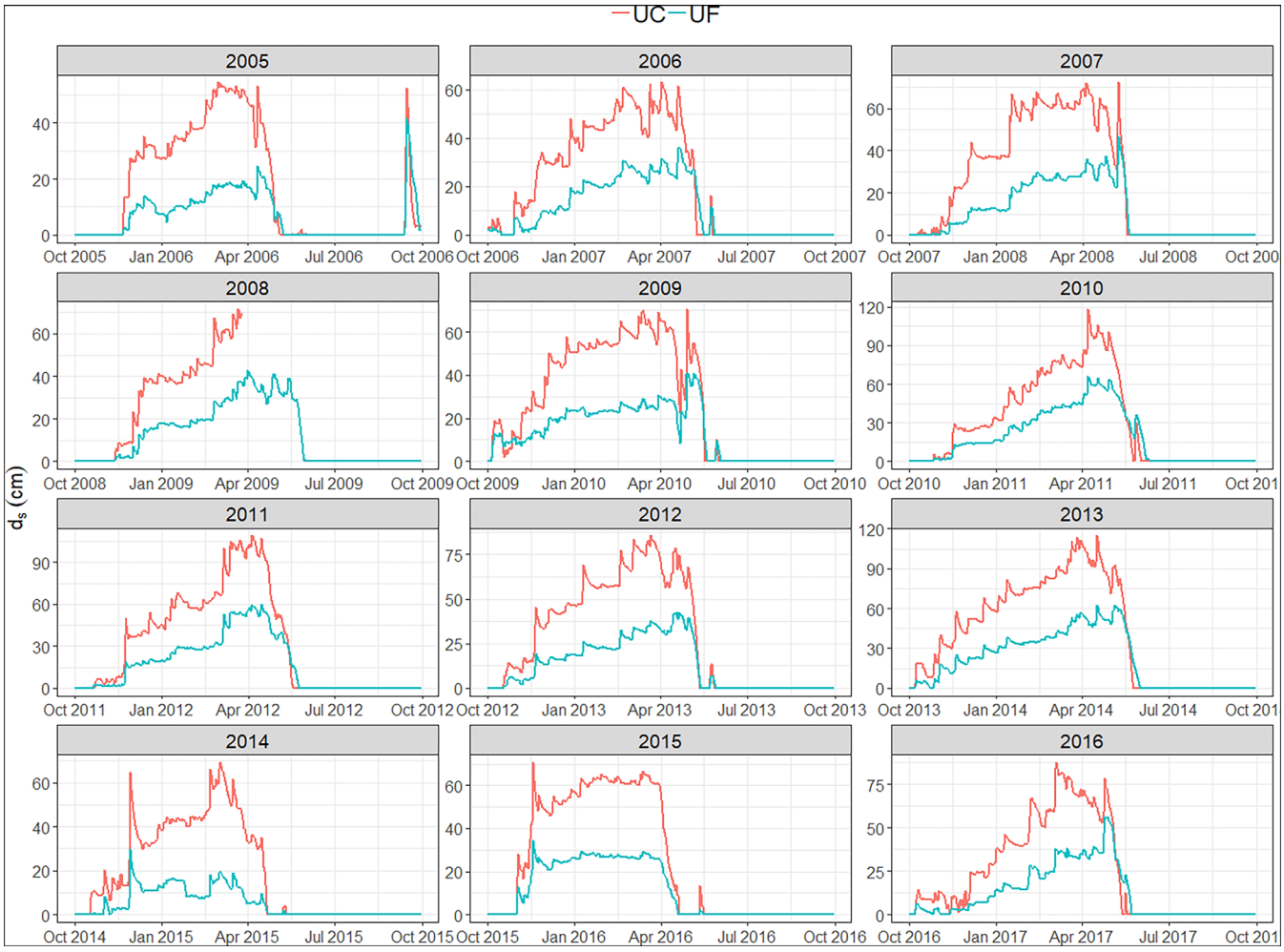

FIGURE 2 SR50 measured snow depth at upper clearing (UC) and upper forest (UF) sites in the Marmot Creek Research Basin

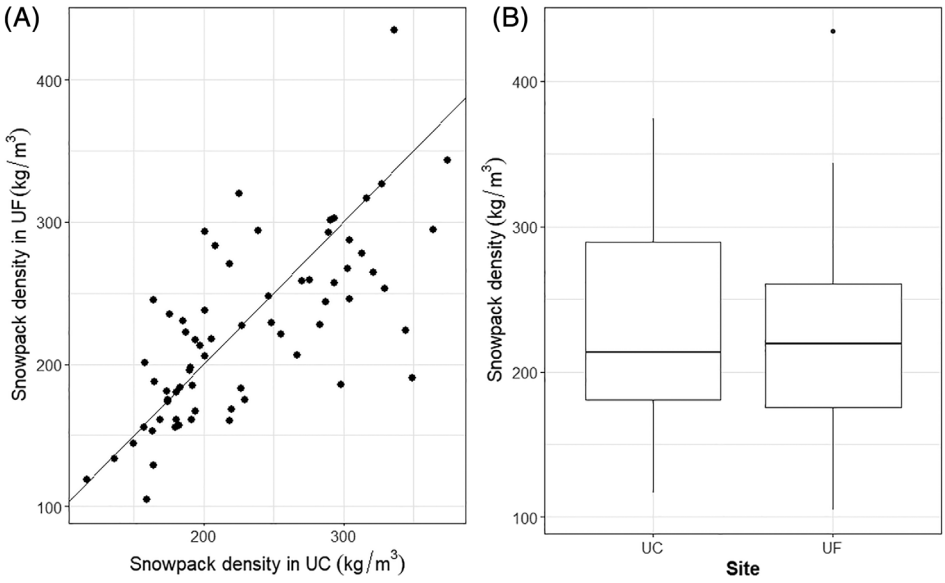

FIGURE 3 Comparison of observed snowpack densities at the upper clearing (UC) and upper forest (UC) sites in Marmot Creek Research Basin. (a) UF density versus UC density and a 1:1 line for comparison, (b) box plots of the distribution and mean of snowpack densities for UF and UC sites

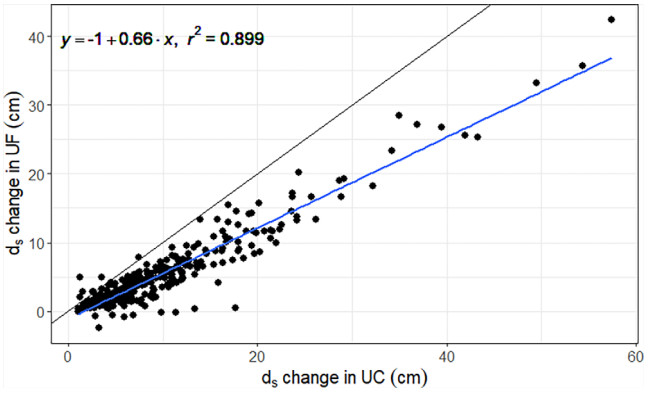

FIGURE 4 Comparison of snow depth (ds) change from upper forest (UF) and upper clearing (UC) during each snowfall event. Black line shows the 1:1 ratio and blue line shows indicates the best linear regression

density at both forest and clearing sites (Figure 5). The overestimation rate was especially high in the early snow season of each hydrological year. On average, the model overestimated snowpack density by 43% at UC and 44% at UF. The RMSE of modelled snowpack density at UC was 130 and 142 kg/m^3 at UF.

Model simulated fresh snow density was frequently higher than that observed, resulting in the modelled snow depth increase being much smaller than that observed (Figure 6). Therefore, using the model simulated snowpack density and observed snow depth leads to the overestimation of SWE at both sites. The calculated fresh snow density using Hedstrom-Pomeroy method was often close to observed while the Jordan et al. method underestimated fresh snow density for both events.

The comparison of calculated and observed fresh snow density for all snowfall events from 2005 to 2017 is shown in Figure 7. The coefficients of determination (r^2) between observed and calculated fresh snow density were lower than 0.4 in both instances. The RMSE of the Hedstrom-Pomeroy equation calculated fresh snow density to be 15 kg/m^3, while the RMSE of the Jordan et al. equation was slightly higher (22 kg/m^3). There was a slight underestimation trend for both the Jordan et al. and Hedstrom-Pomeroy methods; their MB values were −0.02 and −0.08, respectively. The mean value for observed fresh snow density at the UC site was 84 kg/m^3, which is slightly higher than the average value calculated using both methods (82 kg/m^3 [Hedstrom-Pomeroy] and 77 kg/m^3 [Jordan et al.]). The lower limit of calculated fresh snow density, which is the result of low air temperature, was approximately 68 kg/m^3 and 48 kg/m^3 for Hedstrom-Pomeroy and Jordan et al., respectively. This resulted in calculated fresh snow density values for many snowfall events being the same or around the lower limit value. This partially contributed to the relatively low r^2 values in both methods.

The difference between observed and calculated fresh snow density plotted against snow event duration (Figure 8). For the Hedstrom-Pomeroy method, average differences were negative when the snowstorm duration was <12 hr. When the snowstorm duration was longer than 12 hr, the difference became positive, increasing with longer snow event duration, peaking at 57 kg/m^3 when snow event duration was 53 hr. With the Jordan et al. method, average difference values were frequently positive and increasing with longer snow event duration. This indicated that fresh snow densification exists and varies among snow events. This study, and the predictive algorithms tested, assumed that the densification of fresh snow during snow events at sheltered study sites is negligible; a poor assumption for most cold regions (Goodison, Ferguson, & McKay, 1981). However, according to the calculated and observed fresh snow density, the densification rate was frequently less than 1 kg m^{-3}hr^{-1}, indicating that the assumption of little fresh snow densification is valid at present research sites. The densification rate is well correlated to the snow storm duration (Figure 8). Therefore, a small densification rate was added to the calculated fresh snow density for both methods for all snow storms according to the relationship between snow storm duration and

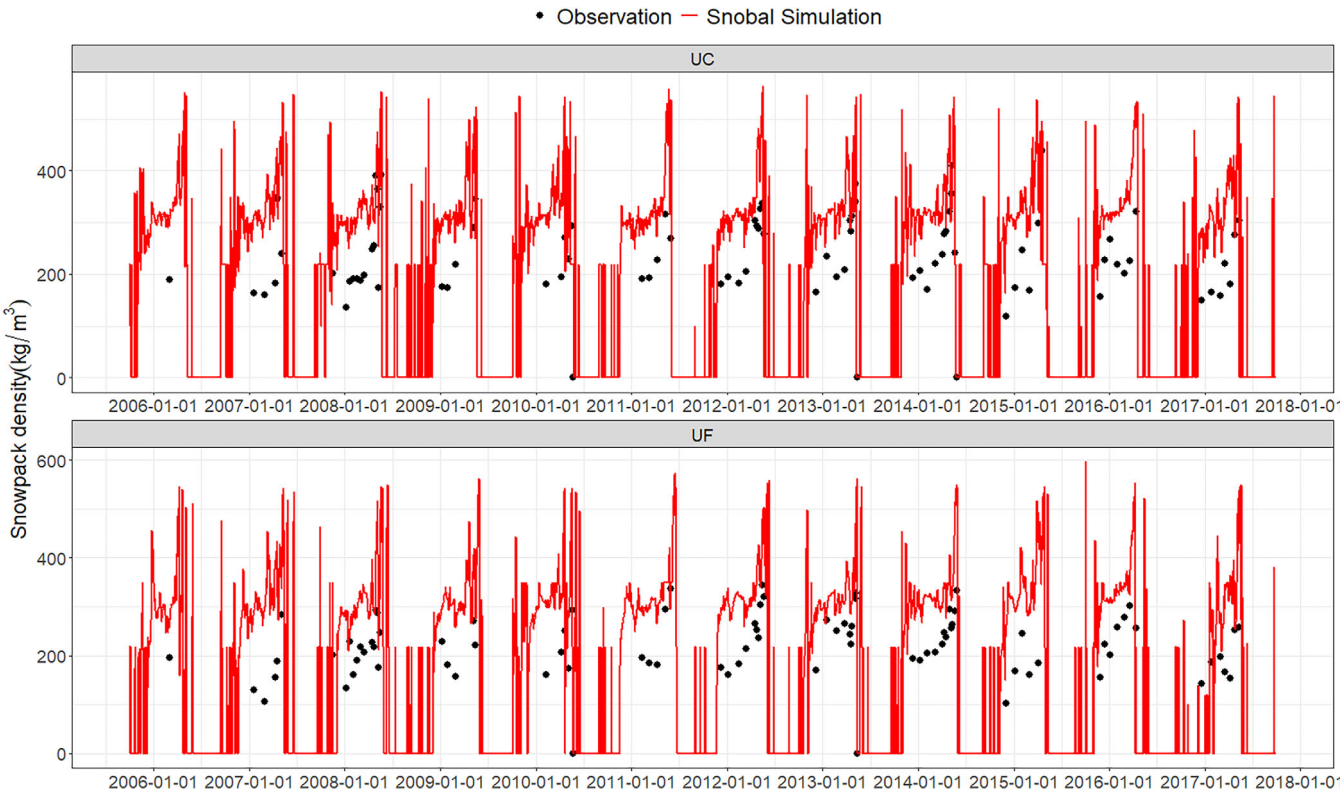

FIGURE 5 Time-series of Snobal-simulated and observed snowpack density in the upper clearing (top) and upper forest (bottom) in Marmot Creek Research Basin

densification rate (Figure 8). In all, the Hedstrom-Pomeroy equation worked better than the Jordan et al. equation at the study sites. In sheltered environments, fresh snow density can be effectively estimated using air temperature and a small densification rate.

4.3 | Validation of interception estimation methods

Calculated snow interception using three methods from 2016 to 2017 was validated using interception data measured by the weighed tree at UF (Figure 9). The Snobal method showed poor accuracy in estimating snow interception with a high RMSE (21.4 mm) and low r^2 (0.21). This may be due to the fact that Snobal largely overestimated the fresh snow density, and hence the SWE, at both sites as it assumes the density of fresh snow is 100 kg/m^3. The two methods that use calculated fresh snow density and observed snow depth increase to estimate SWE change showed greater accuracy. The RMSE of both methods are low (2.0 and 2.6 mm for Hedstrom-Pomeroy and Jordan et al., respectively). The r^2 between calculated and observed snow interception for Hedstrom-Pomeroy method was .72, while the value for Jordan et al. was .66. The Hedstrom-Pomeroy method worked best amongst all methods so it was selected to estimate snow interception at UF. This suggests that continuously measured snow depth data are capable of quantifying snow interception.

4.4 | Snow interception assimilation

Assimilation results were evaluated using upscaled weighed tree measurements and time-lapse camera photos from January to June 2016. These two data sets were both available only during this period. ObsMet-simulated interception magnitude and timing were often close to observations (Figure 10). But the GEM_OL simulated snow interception did not often agree with measurements, while three DA experiments improved interception simulation to varying degrees (Figure 10).

For the snowfall event shown in Figure 10a, the GEM_OL simulated interception began 12 hr earlier than the observation and ended before the observed interception began. The ObsMet simulation slightly overestimated the magnitude and timing of snow interception when compared to observations. All three DA experiments improved the simulation on March 11 and simulated snow interceptions were closer to observations than estimated by ObsMet. However, because assimilation time is midnight, the incorrect interception in the morning of March 10th was not removed and the interception before the midnight was not simulated by all three DAs.

During the event shown in Figure 10b, observations indicated there were only a few hours of snow interception around noon of March 25. The ObsMet simulation agreed with the observation in interception timing but slightly underestimated the interception magnitude. GEM_OL predicted that snow interception was continuous from March 24–26 while the all three DAs did not detect interception

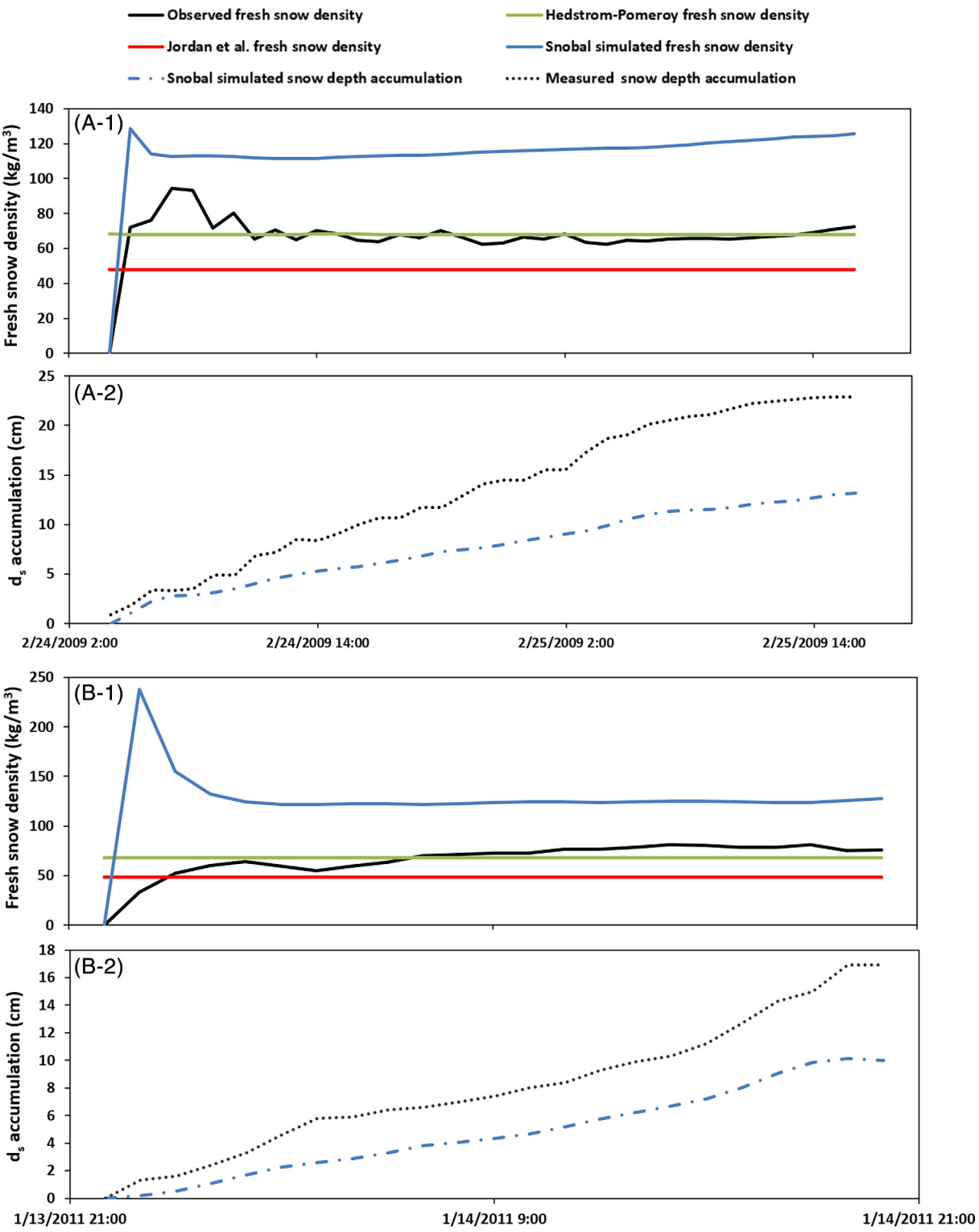

FIGURE 6 Time-series of simulated, calculated, and observed fresh snow density (a-1, b-1) and simulated and observed snow depth accumulation (a-2, b-2) during two snow storms at upper clearing site in Marmot Creek Research Basin

at the beginning of March 25. Simulations of all DAs agreed well with observations for the remaining detected events. However, like GEM_OL, all three DA experiments simulated interception after the March 24th afternoon without improvement of the simulated interception predictions for all three DA experiments on this day.

For the event shown in Figure 10c, snowfall and interception were observed continuously. The ObsMet simulation agreed well with observed interception timing while slightly overestimating the amount of intercepted snow. The GEM_OL simulation did not capture the interception from May 9–10 at all. After assimilation, all three DA

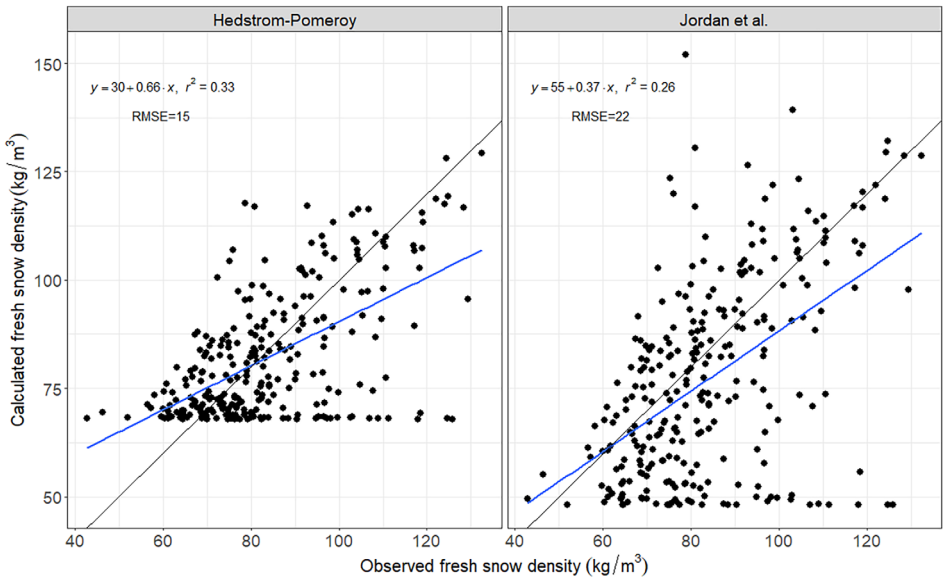

FIGURE 7 Comparison of measured and calculated fresh snow density using Hedstrom-Pomeroy equation (left) and Jordan et al., equation (right) without fresh snow densification at the upper clearing site in Marmot Creek Research Basin. A 1:1 line (black) is plotted for comparison. The regression line (blue) is only shown to display the fitted relationship for the regression

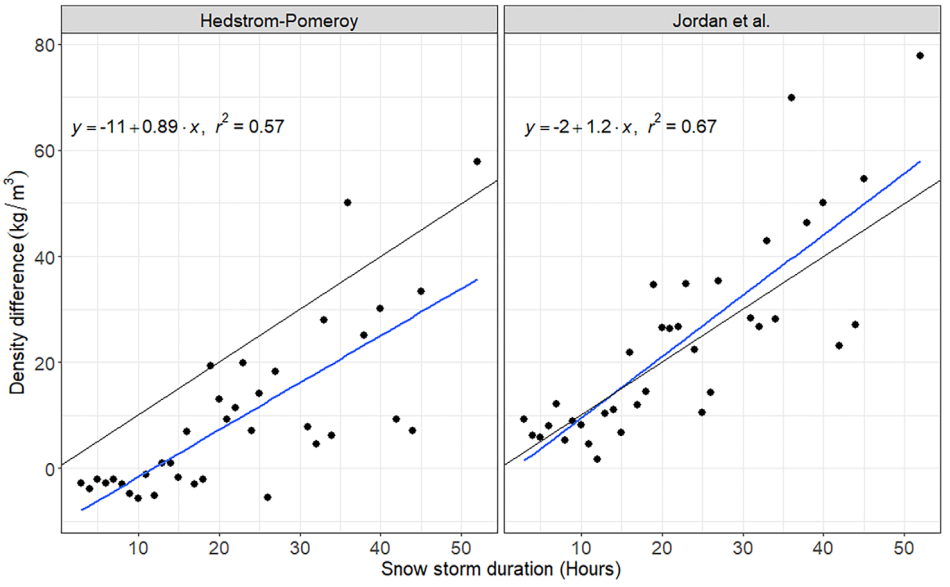

FIGURE 8 Comparison of snow storm duration (hours) to the difference between measured and calculated fresh snow density using two methods at the upper clearing site in Marmot Creek Research Basin. A 1:1 line (black) is plotted for comparison. The regression line (blue) is only shown to display the fitted relationship for the regression

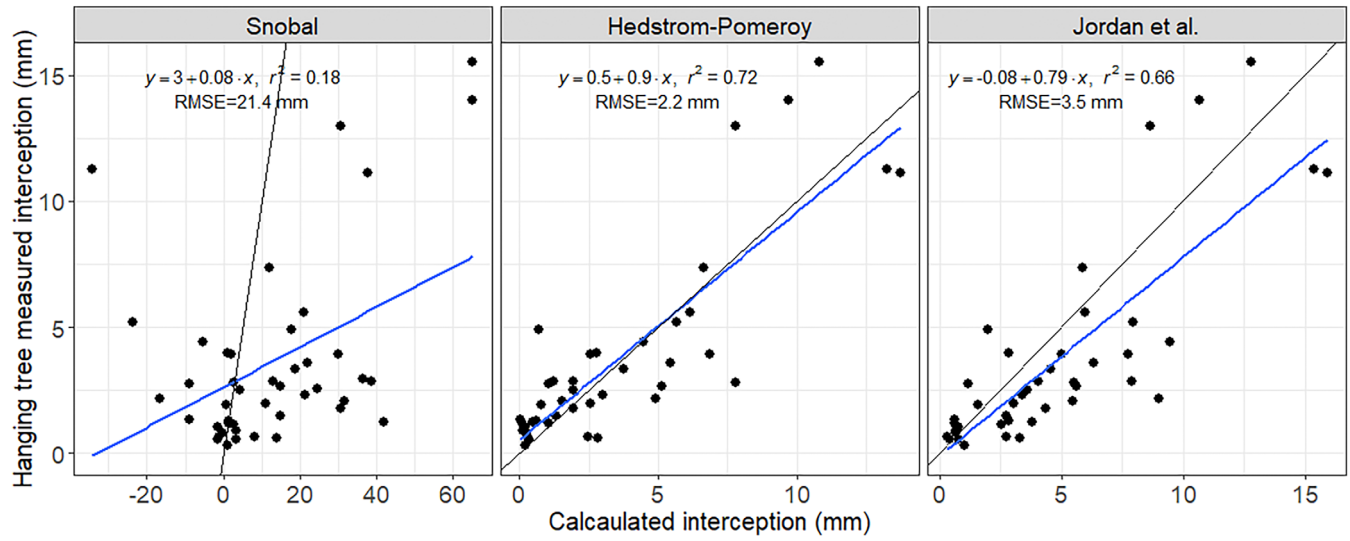

FIGURE 9 Comparisons between snow interception estimated by three methods and weighted tree observations at upper forest site in Marmot Creek Research Basin. A 1:1 comparison line is shown for reference. The regression line (blue) is only shown to display the fitted relationship for the regression

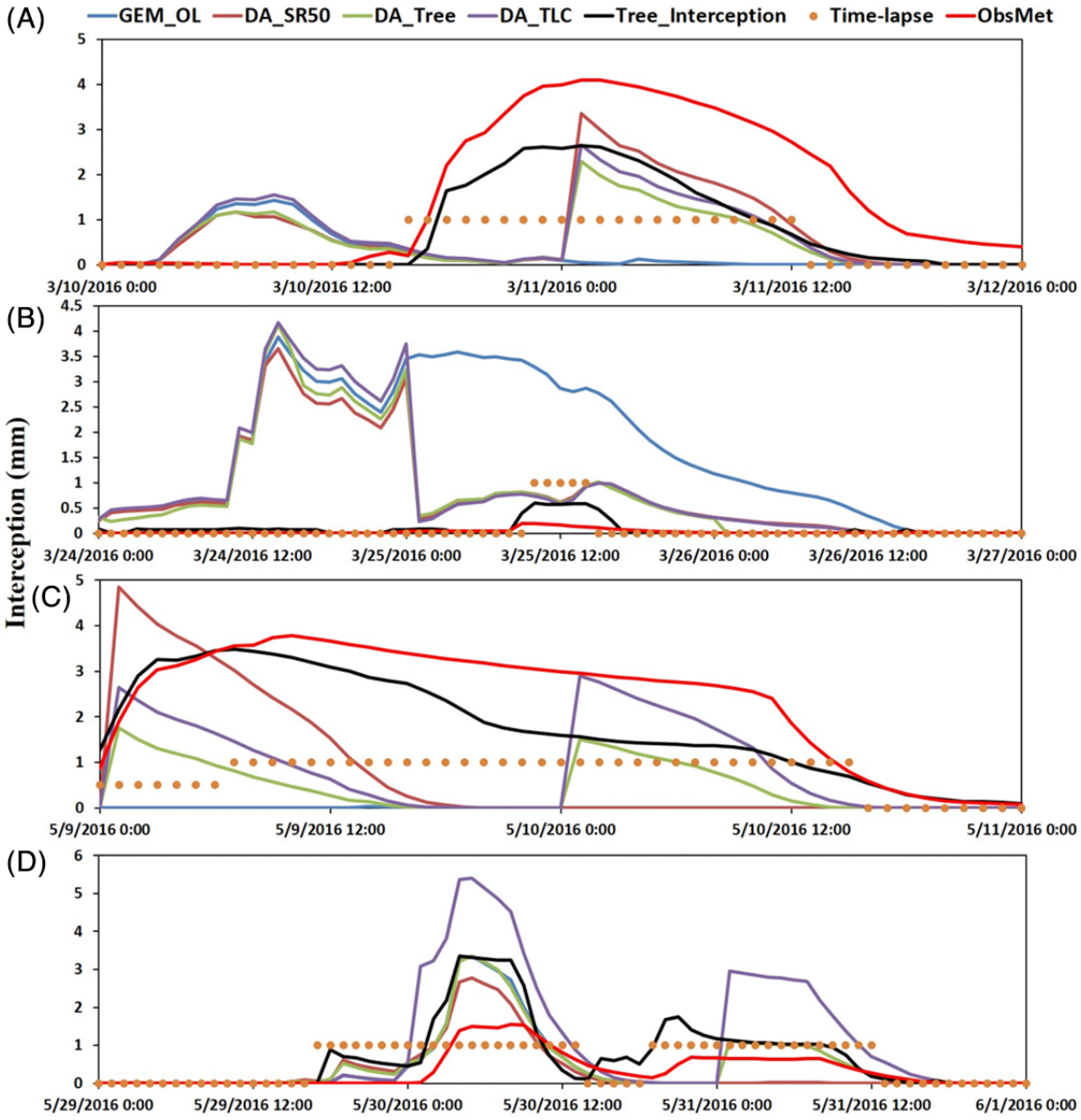

FIGURE 10 Time series of simulated snow interception from different DA experiments driven by GEM data (GEM_OL, DA_SR50, DA_Tree, DA_TLC, unit: mm) and CRHM simulation driven by observed meteorological data (ObsMet, unit: mm), the hanging tree measured snow interception (Tree_Interception, unit: mm), and the time-lapse camera derived canopy snow cover timing (Time-lapse, yellow dot, 0, 1, and 0.5 denote canopy snow free, canopy snow covered, and unknown, respectively)

experiments added some snow to the canopy at the beginning of May 9, but the canopy snow completely ablated in the afternoon that day due to the high simulated sublimation. At the beginning of the May 10th, DA_Tree and DA_TLC added some new snow to the canopy and the simulated canopy snow disappeared earlier than was observed that day. DA_SR50 did not add snow to the canopy on May 10th because this method only assimilates snow interception during a single event without information of how long the snow stays on the canopy.

There were two events shown in Figure 10d. Like previous snowfall events, the ObsMet effectively simulated the timing but not the magnitude of interception. GEM_OL simulated the first event's interception well but missed the second. DA_SR50 and DA_Tree have good simulation results, but DA_TLC greatly overestimated interception during the first event. Because model simulated snow interception was less than 1 mm at the beginning of May 30th, DA_TLC adjusted the snow interception to 3 mm according to assimilation rules. However, because snowfall occurred after midnight, DA_TLC overestimated interception. For the second small event, DA_Tree effectively simulated interception but, again, DA_TLC overestimated it. The DA_SR50 simulation did not add any snow to the canopy because the storm was small and the SR50 interception estimation method did not catch this event.

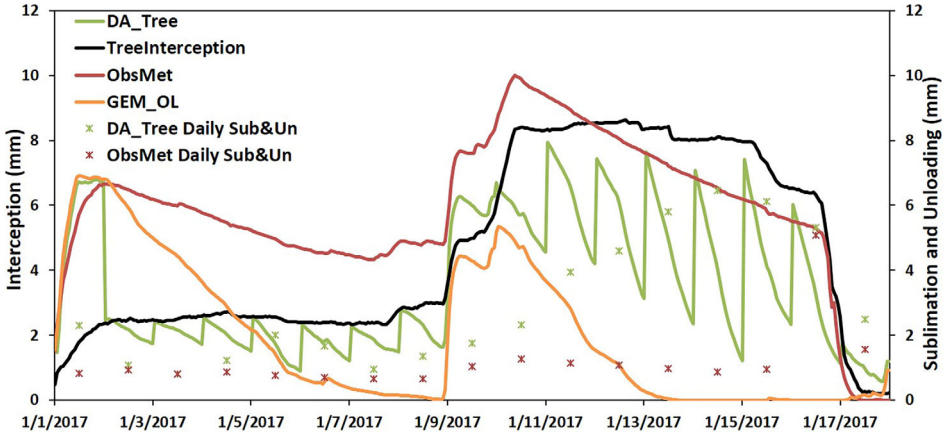

FIGURE 11 Comparison of ObsMet (observation driven), GEM_OL (GEM driven), and DA_Tree (GEM driven) simulated canopy interception to weighed tree measured snow interception (TreeInterception, unit: mm). Stars show the accumulated daily unloading and canopy snow sublimation from DA_Tree and ObsMet simulation (unit: mm)

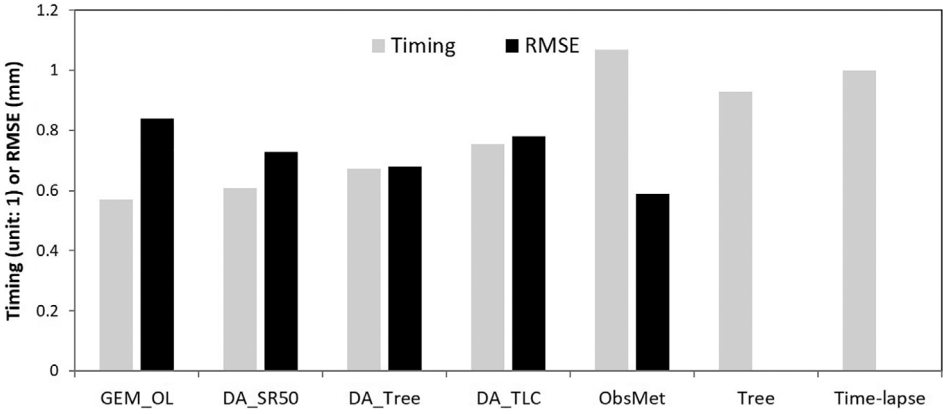

FIGURE 12 Comparison of the performance of different model runs relative to interception measured by a hanging tree and interception timing determined by time-lapse photography. The black bars show RMSE for simulated interception (mm) while the gray bars indicate normalized timing

The unrealistic early depletion of simulated intercepted snow in Figure 10c was largely caused by error in the forcing data. Figure 11 shows an extreme example of how such errors can jeopardize assimilation results. This figure depicts a comparison of canopy snow interception in the ObsMet simulation that is forced by observed meteorological data, to an open loop simulation forced by GEM data; the DA_Tree simulation forced by GEM data and weighed tree measurements. According to the weighed tree measurements, intercepted snow covered the canopy continuously from January 1–17, 2017 and the very little intercepted snow ablated until January 16th. The open loop simulation frequently underestimated canopy snow interception and its simulated interception was not continuous. After assimilation, the DA_Tree simulated interception agreed well with observations at the beginning of each day. However, the model consistently removed the canopy snow by unloading and sublimation after the daily assimilation time until the next assimilation. The ObsMet simulation captured unloading timing well with little error in the interception magnitude. The daily amount of released canopy snow through sublimation and unloading was compared with ObsMet and DA_Tree. The error in GEM forcing data caused a constantly higher ablation rate, mostly due to sublimation, in DA_Tree.

Figure 12 shows the results of DA experiments for the entire validation period. These results illustrate that the suspended tree measurements agreed well with the time-lapse camera data with 93% consistency and ObsMet simulation overestimated interception duration by 4%. However, GEM_OL only agreed with the time-lapse camera information about 57% of the time. After DA, this rate increased to 61, 68, and 76% for DA_SR50, DA_Tree, and DA_TLC, respectively. The improvement of DA_SR50 was small and believed to be caused by the low assimilation frequency. The DA_TLC had the best results indicating that assimilating the time-lapse camera snow interception information based on simple, rule-based method can greatly contribute to predicting interception timing. The RMSE of GEM_OL was 0.84 mm and DA improved the accuracy by varying amounts. DA_Tree (RMSE = 0.68 mm) achieved the best results among all DAs and this likely contributed to its relatively high DA frequency and better input data quality. The improvement in the other two DAs was relatively small, particularly in the case of DA_TLC that only improved accuracy by 0.06 mm. This indicated that although DA_TLC can improve interception timing predictions, its contribution to the simulation magnitude is small.

Although the three DA experiments that were forced using GEM data did not achieve the same results as ObsMet simulation that was forced using local meteorological observations, they all improved the interception magnitude and timing in comparison to the open loop GEM-driven simulation. This indicated that assimilating interception information derived from automatic snow depth measurements and time-lapse cameras into a model that is forced by numerical weather model outputs can achieve results that are similar to those from a model driven by comprehensive, locally observed, forcing data

(without assimilation). As comprehensive meteorological stations are sparse in cold regions forests, this assimilation strategy can benefit interception simulations in these areas.

5 | DISCUSSION

To improve snow interception process simulations through DA, automatically measured snow depth data from a needleleaf forest and adjacent clearings were used to quantify snow interception in the forest canopy. Then, intercepted snow information was assimilated into a physically based hydrological model to better simulate snow interception. Three methods were used to calculate snow density. All were used, along with depth observations, to quantify SWE change during snowfall events both in a forest and a clearing using observed meteorological data. The Hedstrom-Pomeroy fresh snow density equation, using only air temperature to calculate fresh snow density, outperformed other methods. These results agreed with Mair et al. (2016) and Brazenec (2005). Fresh-fallen snow densification can occur immediately after snowfall at a rate of 8–13 kg/m^3·h for up to 12 h during snow events (Goodison et al., 1981). Gray, Norum, and Dyck (1970) also found that the densification rate of snowpack in the Canadian Prairies can reach 9 kg/m^3·h over the course of a blowing snow storm. In the present research, no further densification factor was applied to fresh-fallen snow during snowfall events but the calculated fresh snow density agreed well with observations. Although there was evidence of fresh snow densification when snowfall duration was longer than 12 hours, the densification rate was as low as <1 kg/m^3·h. This is much less than was found by Gray et al. (1970) and Goodison et al. (1981). This is almost certainly due to the fact that the study sites in the present research are located in sheltered environments where wind has a minor influence on snow densification and where cold conditions prevail during snowfall events.

All three DA experiments contribute to better modelling of canopy snow interception. Assimilation of time-lapse camera derived canopy snow information can greatly improve the simulation of canopy snow coverage timing. However, because snow interception is difficult to reliably quantify, improvements to interception magnitude are limited. Overall, the DA_Tree achieved the best results in simulating interception among all three DA experiments. However, the continuous measurement of snow interception from a weighed, suspended tree is not normally available in cold regions forests (there is only one other weighed tree like this in Western Canada). Where data are available, they are confined to a single point in space. Assimilating snow interception information that was derived from continuous snow depth measurements gave reasonable results but with one drawback; it provides snow interception at the end of a snowfall event but not information on canopy snow coverage duration. This method has a lower DA frequency and no control on the snow unloading process compares to the other two DAs.

All three methods share a constraint that originates with the CRHM model. Because CRHM can only export and read the state file at the beginning of each day, the highest assimilation frequency has a 24-hour return interval. This is not a significant issue for surface snowpack assimilation (Lv, 2019), but greatly influences canopy snow estimation. Unlike the surface snowpack that remains on the ground from weeks to months, snow intercepted in forest canopies lasts only from hours to tens of days. If canopy snow storage is ephemeral, then a daily assimilation period is too infrequent to obtain useful information (cf. Figures 10a,b,d). Therefore, higher assimilation frequencies at sub-daily or even hourly rates are preferable for canopy intercepted snow DA.

Due to canopy snow interception processes, DA results may not be accurate even if reliable observations of snow interception are available. Compared to snow on the ground, canopy intercepted snow amounts are small and coverage is transitory, persisting for a shorter time and making it very sensitive to meteorological conditions. In modelling deep surface snowpacks, a minor error in the forcing data (e.g., temperature and humidity) usually does not significantly alter estimates. However, canopy snow interception storage is often less than 10 mm. Thus, forcing data errors can significantly influence simulation results, reducing the benefits of DA. Even in examples when canopy snow interception was rapidly updated as in the DA_Tree experiment (Figures 10c and 11), the canopy snow quickly unloaded each day after assimilations. This indicates that although DA can improve interception simulations during, or shortly after, the assimilation period, this improvement would be short-lived if the model is run using poor quality forcing data.

DA is most often employed with conceptual or operational hydrological models to improve streamflow forecasts. Here it is used to improve the simulation of a hydrological process as part of a physically based hydrological model driven by an atmospheric model. This shows that DA can be used to overcome uncertainty in atmospheric model forcing data and to permit the application of process hydrology calculations in data sparse regions. This can increase the uptake and application of process hydrology models for practical applications and shows the potential to make greater use of snow depth observations that are becoming available from snow stations, and airborne and UAV-borne LiDAR observations.

6 | CONCLUSIONS

To achieve a better estimates of snow interception process magnitude and timing, a DA approach was used in this research. Automatically measured snow depth data from an adjacent needleleaf forest and clearing were analyzed to quantify losses due to forest canopy snow interception. Peak snow depth in the forest was on average approximately 46% lower than in the clearing. During snowfall events, snow accumulation under the forest canopy was approximately 48% less than that in the clearing. Three fresh snow density estimation methods were tested, with results indicating that the Hedstrom-Pomeroy equation using air temperature to calculate fresh snow density worked best. Combining measured snow depth data with calculated fresh snow density, snow interception was determined for each snow event. Calculated snow interception using this technique agreed

well with measurements from a weighed, suspended tree. This indicated that automatically measured snow depths from adjacent forests and clearings are suitable to estimate snow interception in the forest canopy.

This study has attempted to assimilate snow interception information into a hydrological process model for the first time. Calculated snow interception from automated snow depth data, along with suspended tree and time-lapse camera measured snow interception data, were assimilated into the Cold Regions Hydrological Model, driven by GEM atmospheric model outputs, using the EnKF or rule-based direct insertion approaches. Although these simulations after DA were not as accurate as models driven by locally observed meteorology, they all improved the simulation accuracy of snow interception amount and timing. Due to the relatively small magnitude of intercepted snow in the canopy, snow interception DA is greatly influenced by the assimilation quality of forcing data. The benefit of assimilation does not last long if the quality of forcing data is poor. Interception assimilation results are also heavily influenced by assimilation frequency. Daily assimilation frequencies can achieve accurate results, but sub-daily or hourly frequencies are more effective for intercepted snow DA. Owing to sparse data availability and size of study site, this research assimilated information at a forest stand scale. With the development of satellite and UAV-based remote sensing, increasing large scale snow interception estimation can become available. The addition of these measures should improve canopy snow interception simulation and cold regions water resource management.

ACKNOWLEDGMENTS

The authors would like to acknowledge the remarkable contributions of Mr Tom Brown to the development and coding of CRHM over 21 years. The support from Xing Fang and Nicholas Wayand on CRHM model project and forcing data collection are much appreciated. Funding from the Natural Sciences and Engineering Research Council of Canada, the Changing Cold Regions Network, the Canada Excellence Research Chair in Water Security, the Canada Research Chairs Program, Alberta Innovates, Alberta Agriculture and Forestry, and the Global Water Futures Program made this study possible. The cooperation and logistical assistance of the Nakiska Ski Resort in operation of MCRB and field observations from May Guan, Angus Duncan, and Greg Galloway and many students and researchers provided the observational basis for this study.

DATA AVAILABILITY STATEMENT

The data used are listed in the references, tables and figures in this paper and can be also found at: http://www.ccrnetwork.ca/outputs/data/index.php.

ORCID


Zhibang Lv https://orcid.org/0000-0003-1476-8902

REFERENCES

Andreadis, K. M., & Lettenmaier, D. P. (2006). Assimilating remotely sensed snow observations into a macroscale hydrology model. *Advances in Water Resources*, *29*, 872–886. https://doi.org/10.1016/j.advwatres.2005.08.004

Bales, R. C., Hopmans, J. W., O'Geen, A. T., Meadows, M., Hartsough, P. C., Kirchner, P., … Beaudette, D. (2011). Soil moisture response to snowmelt and rainfall in a Sierra Nevada mixed-conifer forest. *Vadose Zone Journal*, *10*, 786–799. https://doi.org/10.2136/vzj2011.0001

Bartlett, P. A., MacKay, M. D., & Verseghy, D. L. (2006). Modified snow algorithms in the Canadian land surface scheme: Model runs and sensitivity analysis at three boreal forest stands. *Atmosphere – Ocean*, *44*, 207–222. https://doi.org/10.3137/ao.440301

Bergeron, J. M., Trudel, M., & Leconte, R. (2016). Combined assimilation of streamflow and snow water equivalent for mid-term ensemble streamflow forecasts in snow-dominated regions. *Hydrology and Earth System Sciences*, *20*, 4375–4389. https://doi.org/10.5194/hess-20-4375-2016

Brazenec, W. A. (2005). *Evaluation of ultrasonic snow depth sensors for automated surface observing systems (ASOS)*. (Unpublished MS thesis). Colorado State University, Fort Collins, CO, p. 124.

Campbell Scientific (2009). *SR50A sonic ranging sensor, instruction manual* (p. 42). Logan, UT: Campbell Scientific Canada Corp.

Clark, M. P., Slater, A. G., Barrett, A. P., Hay, L. E., McCabe, G. J., Rajagopalan, B., & Leavesley, G. H. (2006). Assimilation of snow covered area information into hydrologic and land-surface models. *Advances in Water Resources*, *29*, 1209–1221. https://doi.org/10.1016/j.advwatres.2005.10.001

DeBeer, C. M., & Pomeroy, J. W., (2010). Simulation of the snow melt runoff contributing area in a small alpine basin. *Hydrology and Earth System Sciences*, *14*,1205–1219. https://doi.org/10.5194/hess-14-1205-2010.

De Lannoy, G. J. M., Reichle, R. H., Arsenault, K. R., Houser, P. R., Kumar, S., Verhoest, N. E. C., & Pauwels, V. R. N. (2012). Multiscale assimilation of Advanced Microwave Scanning Radiometer-EOS snow water equivalent and Moderate Resolution Imaging Spectroradiometer snow cover fraction observations in northern Colorado. *Water Resources Research*, *48*, W01522. https://doi.org/10.1029/2011wr010588

Egli, L., Jonas, T., & Meister, R. (2009). Comparison of different automatic methods for estimating snow water equivalent. *Cold Regions Science and Technology*, *57*(2–3), 107–115. https://doi.org/10.1016/j.coldregions.2009.02.008

Ellis, C. R., Pomeroy, J. W., Brown, T., & MacDonald, J. P. (2010). Simulation of snow accumulation and melt in needleleaf forest environments. *Hydrology and Earth System Sciences*, *14*, 925–940. https://doi.org/10.5194/hess-14-925-2010

Fang, X., & Pomeroy, J. W. (2016). Impact of antecedent conditions on simulations of a flood in a mountain headwater basin. *Hydrological Processes*, *30*, 2754–2772. https://doi.org/10.1002/hyp.10910

Fang, X., Pomeroy, J. W., DeBeer, C. M., Harder, P., & Siemens, E. (2019). Hydrometeorological data from Marmot Creek Research Basin, Canadian Rockies. *Earth System Science Data*, *11*, 455–471. https://doi.org/10.5194/essd-11-455-2019

Fang, X., Pomeroy, J. W., Ellis, C. R., MacDonald, M. K., DeBeer, C. M., & Brown, T. (2013). Multi-variable evaluation of hydrological model predictions for a headwater basin in the Canadian Rocky Mountains. *Hydrology and Earth System Sciences*, *17*, 1635–1659. https://doi.org/10.5194/hess-17-1635-2013

Floyd, W., & Weiler, M. (2008). Measuring snow accumulation and ablation dynamics during rain-on-snow events: Innovative measurement techniques. *Hydrological Processes*, *22*, 4805–4812. https://doi.org/10.1002/hyp.7142

Franz, K. J., Hogue, T. S., Barik, M., & He, M. (2014). Assessment of SWE data assimilation for ensemble streamflow predictions. *Journal of Hydrology*, *519*, 2737–2746. https://doi.org/10.1016/j.jhydrol.2014.07.008

Friesen, J., Lundquist, J., & Van Stan, J. T. (2015). Evolution of forest precipitation water storage measurement methods. *Hydrological Processes*, *29*, 2504–2520. https://doi.org/10.1002/hyp.10376

Garvelmann, J., Pohl, S., & Weiler, M. (2013). From observation to the quantification of snow processes with a time-lapse camera network. *Hydrology and Earth System Sciences*, *17*, 1415–1429. https://doi.org/10.5194/hess-17-1415-2013

Goodison, B. E., Ferguson, H. L., & McKay, G. A. (1981). Measurement and data analysis. In D. M. Gray, & D. H. Male (Eds.), *Handbook of snow: Principles, processes, management and use* (pp. 191–274). New York, NY: Pergamon Press.

Gray. D. M., Norum, D. I., & Dyck. G. E. (1970). *Densities of prairie snowpacks*. Proc. 38th Annual Meeting Western Snow Conference. pp. 24–30.

Harder, P., & Pomeroy, J. W. (2013). Estimating precipitation phase using a phycrometric energy balance method. *Hydrological Processes*, *27*, 1901–1914. https://doi.org/10.1002/hyp.9799

He, M., Hogue, T. S., Margulis, S. A., & Franz, K. J. (2012). An integrated uncertainty and ensemble-based data assimilation approach for improved operational streamflow predictions. *Hydrology and Earth System Sciences*, *16* (3), 815–831. https://doi.org/10.5194/hess-16-815-2012

Hedrick, A. R., Marks, D., Havens, S., Robertson, M., Johnson, M., Sandusky, M., … Painter, T. H. (2018). Direct insertion of NASA Airborne Snow Observatory-derived snow depth time series into the iSnobal energy balance snow model. *Water Resources Research*, *54*. https://doi.org/10.1029/2018WR023190, 8045–8063.

Hedstrom, N. R., & Pomeroy, J. W. (1998). Measurements and modelling of snow interception in the boreal forest. *Hydrological Processes*, *12*, 1611–1625. https://doi.org/10.1002/(SICI)1099-1085(199808/09)12:10/11<1611::AID-HYP684>3.0.CO;2-4

Helfricht, K., Hartl, L., Koch, R., Marty, C., & Olefs, M. (2018). Obtaining sub-daily new snow density from automated measurements in high mountain regions. *Hydrology and Earth System Sciences*, *22*(5), 2655. https://doi.org/10.5194/hess-22-2655-2018–2668.

Huang, C. C., Newman, A. J., Clark, M. P., Wood, A. W., & Zhang, X. (2017). Evaluation of snow data assimilation using the ensemble Kalman filter for seasonal streamflow prediction in the western United States. *Hydrology and Earth System Sciences*, *21*, 635–650. https://doi.org/10.5194/hess-21-635-2017

Jordan, R. E., Andreas, E. L., & Makshtas, A. P. (1999). Heat budget of snow-covered sea ice at North Pole 4. *Journal of Geophysical Research*, *104*(C4), 7785–7806. https://doi.org/10.1029/1999JC900011

Kinar, N. J., & Pomeroy, J. W. (2015). Measurement of the physical properties of the snowpack. *Reviews of Geophysics*, *53*(2), 481–544. https://doi.org/10.1002/2015RG000481

Koivusalo, H., & Kokkonen, T. (2002). Snow processes in a forest clearing and in a coniferous forest. *Journal of Hydrology*, *262*(1–4), 145–164. https://doi.org/10.1016/S0022-1694(02)00031-8

Kumar, S., Koster, R., Crow, W., & Peters-Lidard, C. (2009). Role of subsurface physics in the assimilation of surface soilmoisture observations. *Journal of Hydrometeorology*, *10*, 1534–1547. https://doi.org/10.1175/2009JHM1134.1

Kumar, S., Peters-Lidard, C., Mocko, D., Reichle, R., Liu, Y., Arsenault, K., … Cosh, M. (2014). Assimilation of remotely sensed soil moisture and snow depth retrievals for drought estimation. *Journal of Hydrometeorology*, *15*, 2446–2469. https://doi.org/10.1175/JHM-D-13-0132.1

Kumar, S. V., Dong, J., Peters-Lidard, C. D., Mocko, D., & Gómez, B. (2017). Role of forcing uncertainty and background model error characterization in snow data assimilation. *Hydrology and Earth System Sciences*, *21* (6), 2637–2647. https://doi.org/10.5194/hess-21-2637-2017

Kuz'min, P.P., (1960). *Formirovanie Snezhnogo Pokrova i Metody Opredeleniya Snegozapasov*. In: Gidrometeoizdat: Leningrad. Published 1963 as Snow Cover and Snow Reserves. National Science Foundation, Washington, DC, pp. 139 [English Translation by Israel Program for Scientific Translation, Jerusalem].

Liston, G. E., & Hiemstra, C. A. (2007). A simple data assimilation system for complex snow distributions (SnowAssim). *Journal of Hydrometeorology*, 989–1004. https://doi.org/10.1175/2008JHM871.1

Liu, Y., Peters-Lidard, C., Kumar, S., Foster, J., Shaw, M., Tian, Y., & Fall, G. (2013). Assimilating satellite-based snow depth and snow cover products for improving snow predictions in Alaska. *Advances in Water Resources*, *54*, 208–227. https://doi.org/10.1016/j.advwatres.2013.02.005

Liu, Y., Weerts, A. H., Clark, M., Hendricks Franssen, H.-J., Kumar, S., Moradkhani, H., … Restrepo, P. (2012). Advancing data assimilation in operational hydrologic forecasting: Progresses, challenges, and emerging opportunities. *Hydrology and Earth System Sciences*, *16*, 3863–3887. https://doi.org/10.5194/hess-16-3863-2012

Lundberg, A., Calder, I., & Harding, R. (1998). Evaporation of intercepted snow: Measurement and modelling. *Journal of Hydrology*, *206*(3–4), 151–163. https://doi.org/10.1016/S0022-1694(97)00016-4

Lv, Z., & Pomeroy, J. W. (2019). Detecting intercepted snow in the coniferous forest by using satellite remotely sensed data. *Remote Sensing of Environment*, *231*. https://doi.org/10.1016/j.rse.2019.111222

Lv, Z. (2019). Assimilation of snow information into cold regions hydrological model. PhD thesis. Saskatoon, Canada: University of Saskatchewan.

Lv, Z., Pomeroy, J. W., & Fang, X. (2019). Evaluation of SNODAS snow water equivalent in western Canada and assimilation into a Cold Region Hydrological Model. *Water Resources Research*, *55*, 11166–11187. https://doi.org/10.1029/2019WR025333

Magnusson, J., Winstral, A., Stordal, A. S., Essery, R., & Jonas, T. (2017). Improving physically based snow simulations by assimilating snow depths using the particle filter. *Water Resources Research*, *53*, 1125–1143. https://doi.org/10.1002/2016WR019092

Mair, E., Leitinger, G., Della Chiesa, S., Niedrist, G., Tappeiner, U., & Bertoldi, G. (2016). A simple method to combine snow height and meteorological observations to estimate winter precipitation at sub-daily resolution. *Hydrological Sciences Journal*, *61*(11), 2050–2060. https://doi.org/10.1080/02626667.2015.1081203

Marks, D., Kimball, J., Tingey, D., & Link, T. (1998). The sensitivity of snowmelt processes to climate conditions and forest cover during rain-on-snow: A case study of the 1996 Pacific Northwest flood. *Hydrological Processes*, *12*, 1569–1587. https://doi.org/10.1002/(SICI)1099-1085(199808/09)12:10/11<1569::AID-HYP682>3.0.CO;2-L

Marks, D., Reba, M., Pomeroy, J. W., Link, T. E., Winstral, A., Flerchinger, G., & Elder, K. (2008). Comparing simulated and measured sensible and latent heat fluxes over snow under a pine canopy to improve an energy balance snowmelt model. *Journal of Hydrometeorology*, *9*, 1506–1522. https://doi.org/10.1175/2008JHM874.1

Martin, K. A., Van Stan, J. T., Dickerson-Lange, S. E., Lutz, J. A., Berman, J. W., Gersonde, R., & Lundquist, J. D. (2013). Development and testing of a snow interceptometer to quantify canopy water storage and interception processes in the rain/snow transition zone of the North Cascades, Washington, USA. *Water Resources Research*, *49*, 3243–3256. https://doi.org/10.1002/wrcr.20271

Neumann, N. N., Derksen, C., Smith, C., & Goodison, B. (2006). Characterizing local scale snow cover using point measurements during the winter season. *Atmosphere Ocean*, *44*(3), 257–269. https://doi.org/10.3137/ao.440304

Niu, G.-Y., & Yang, Z.-L. (2004). Effects of vegetation canopy processes on snow surface energy and mass balances. *Journal of Geophysical Research*, *109*, D23111. https://doi.org/10.1029/2004JD004884

Painter, T. H., Berisford, D. F., Boardman, J. W., Bormann, K. J., Deems, J. S., Gehrke, F., … Winstral, A. (2016). The Airborne Snow Observatory: Fusion of scanning lidar, imaging spectrometer, and physically-based modeling for mapping snow water equivalent and snow albedo. *Remote Sensing of Environment*, *184*, 139–152. https://doi.org/10.1016/j.rse.2016.06.018

Parviainen, J., & Pomeroy, J. W. (2000). Multiple-scale modelling of forest snow sublimation: Initial findings. *Hydrological Processes*, *14*, 2669–2681. https://doi.org/10.1002/1099-1085(20001030)14:15<2669::AID-HYP85>3.0.CO;2-Q

Pomeroy, J. W., & Dion, K. (1996). Winter radiation extinction and reflection in a boreal pine canopy: Measurements and modelling. *Hydrological Processes*, *10*, 1591–1608. https://doi.org/10.1002/(SICI)1099-1085(199612)10:12<1591::AID-HYP503>3.0.CO;2-8

Pomeroy, J. W., Fang, X., & Ellis, C. (2012). Sensitivity of snowmelt hydrology in Marmot Creek, Alberta, to forest cover disturbance. *Hydrological Processes*, *26*, 1891–1904. https://doi.org/10.1002/hyp.9248

Pomeroy, J. W., Fang, X., & Marks, D. G. (2016). The cold rain-on-snow event of June 2013 in the Canadian Rockies - Characteristics and diagnosis. *Hydrological Processes*, *30*, 2899–2914. https://doi.org/10.1002/hyp.10905

Pomeroy, J. W., & Goodison, B. E. (1997). Winter and snow. In W. G. Bailey, T. R. Oke, & W. R. Rouse (Eds.), *The surface climates of Canada* (pp. 68–100). Montreal: McGillQueen's University Press. https://doi.org/10.1023/a:1001753810703

Pomeroy, J. W., & Gray, D. M. (1995). *Snowcover accumulation, relocation and management*. NHRI Science Report No. 7. National Hydrology Research Institute, Environment Canada, Saskatoon. p. 134.

Pomeroy, J. W., Gray, D. M., Brown, T., Hedstrom, N. R., Quinton, W. L., Granger, R. J., & Carey, S. K. (2007). The cold regions hydrological process representation and model: A platform for basing model structure on physical evidence. *Hydrological Processes*, *21*, 2650–2667. https://doi.org/10.1002/hyp.6787

Pomeroy, J. W., Gray, D. M., Shook, K. R., Toth, B., Essery, R. L. H., Pietroniro, A., & Hedstrom, N. R. (1998). An evaluation of snow accumulation and ablation processes for land surface modelling. *Hydrological Processes*, *12*, 2339–2367. https://doi.org/10.1002/(SICI)1099-1085(199812)12:15

Pomeroy, J. W., Rowlands, A., Hardy, J., Link, T. E., Marks, D., Essery, R. L. H., … Ellis, C. R. (2008). Spatial variability of shortwave irradiance for snowmelt in forests. *Journal of Hydrometeorology*, *9*, 1482–1490. https://doi.org/10.1175/2008JHM867.1

Pomeroy, J. W., & Schmidt, R. A. (1993). The use of fractal geometry in modeling intercepted snow accumulation and sublimation. *Proceedings of the Eastern Snow Conference*, *50*, 1–10.

Pomeroy, J. W., Gray, D. M., Hedstrom, N. R., & Janowicz, J.R., (2002). Prediction of seasonal snow accumulation in cold climate forests. *Hydrological Processes*, *16*,3543–3558. https://doi.org/10.1002/hyp.1228.

Reichle, R. H., Koster, R. D., Liu, P., Mahanama, S. P. P., Njoku, E. G., & Owe, M. (2007). Comparison and assimilation of global soil moisture retrievals from the Advanced Microwave Scanning Radiometer for the Earth Observing System (AMSR-E) and the Scanning Multichannel Microwave Radiometer (SMMR). *Journal of Geophysical Research-Atmospheres*, *112*(D9), D09108. https://doi.org/10.1029/2006JD008033

Reichle, R. H., Walker, J. P., Koster, R. D., & Houser, P. R. (2002). Extended versus ensemble Kalman filtering for land data assimilation. *Journal of Hydrometeorology*, *3*, 728–740. https://doi.org/10.1175/1525-7541(2002)003<0728:EVEKFF>2.0.CO;2

Rodell, M., & Houser, P. R. (2004). Updating a land surface model with MODIS-derived snow cover. *Journal of Hydrometeorology*, *5*, 1064–1075. https://doi.org/10.1175/JHM-395.1

Rothwell, R., Hillman, G., & Pomeroy, J. W. (2016). Marmot creek experimental watershed study. *The Forestry Chronicle*, *92*, 32–36. https://doi.org/10.5558/tfc2016-010

Ryan, W. A., Doesken, N. J., & Fassnacht, S. R. (2008). Evaluation of ultrasonic snow depth sensors for US snow measurements. *Journal of Atmospheric and Oceanic Technology*, *25*(5), 667–684. https://doi.org/10.1175/2007JTECHA947.1

Schmidt, R. A., & Pomeroy, J. W. (1990). Bending of a conifer branch at subfreezing temperatures: Implications for snow interception. *Canadian Journal of Forest Research*, *20*, 1250–1253. https://doi.org/10.1139/x90-165

Slater, A. G., & Clark, M. P. (2006). Snow data assimilation via an ensemble Kalman filter. *Journal of Hydrometeorology*, *7*, 478–493. https://doi.org/10.1175/jhm505.1

Smith, C. D. (2009). *The relationship between snowfall catch efficiency and wind speed for the Geonor T-200B precipitation gauge utilizing various wind shield configurations*. Proceedings of the 77th Western Snow Conference, Canmore AB, pp. 115–121.

Stigter, E. E., Wanders, N., Saloranta, T. M., Shea, J. M., Bierkens, M. F. P., & Immerzeel, W. W. (2017). Assimilation of snow cover and snow depth into a snow model to estimate snow water equivalent and snowmelt runoff in a Himalayan catchment. *The Cryosphere*, *11*, 1647–1664. https://doi.org/10.5194/tc-11-1647-2017

Storck, P., Lettenmaier, D. P., & Bolton, S. (2002). Measurement of snow interception and canopy effects on snow accumulation and melt in mountainous maritime climate, Oregon, USA. *Water Resources Research*, *38*, 1223–1238. https://doi.org/10.1029/2002WR001281

Suzuki, K., & Nakai, Y. (2008). Canopy snow influence on water and energy balances in a coniferous forest plantation in northern Japan. *Journal of Hydrology*, *352*, 126–138. https://doi.org/10.1016/j.jhydrol.2008.01.007

Winkler, R. D., Spittlehouse, D. L., & Golding, D. L. (2005). Measured differences in snow accumulation and melt among clearcut, juvenile, and mature forests in southern British Columbia. *Hydrological Processes*, *19*(1), 51–62. https://doi.org/10.1002/hyp.5757

How to cite this article: Lv Z, Pomeroy JW. Assimilating snow observations to snow interception process simulations. *Hydrological Processes*. 2020;1–18. https://doi.org/10.1002/hyp.13720